Metals and Materials International (2022) 28:1433–1444
https://doi.org/10.1007/s12540-021-01009-3

Microstructure Evolution, Mechanical Properties and Strain Hardening Instability of Low and Medium Carbon Quenching & Partitioning Steels

Ramadan N. Elshaer[1] · Mohamed K. El-Fawakhry[2] · Ahmed I. Z. Farahat[3]

Received: 16 January 2021 / Accepted: 4 March 2021 / Published online: 5 August 2021

Abstract
The effect of quenching after martensitic finish (QAM_f) or quenching & partitioning (Q&P) on microstructure evolution, mechanical properties, and strain hardening instability of low and medium carbon hot rolled steels were investigated. Two heats of low and medium carbon steels were cast in an induction open furnace. The chemical composition of low carbon steel is 0.16C–0.27Si–1.47Mn–0.02Al while medium carbon steel is 0.49C–0.30Si–0.91Mn–0.03Al. They were hot-rolled at 1200 °C for 30 min followed by air cooling. The microstructure after hot-rolled gives bands of ferrite and pearlite for 0.16 wt% low carbon steel. On the other hand, 0.49 wt% medium carbon steel produces coarse pearlite islands surrounded by ferrite phase. To enhance mechanical properties, it was necessary to modify the microstructure of low and medium carbon steels using QAM_f or Q&P processes. The resultant matrix of microstructure after QAM_f and Q&P processes contained ferrite, bainite, lath martensite, and retained austenite for 0.16 wt% low carbon steel, and polygonal ferrite, lath martensite, and retained austenite for 0.49 wt% medium carbon steel, respectively. In low carbon steel, QAM_f process increased uniform elongation from 6.6 to 13.5% (105% increase) while ultimate tensile strength (UTS) improved slightly from 645 to 692 MPa (7% increase). However, in medium carbon steel, Q&P reduced uniform elongation from 12.4 to 4.8% (61% decrease) while increased UTS from 769 to 1242 MPa (61.5% increase). It is worthy to mention that QAM_f process exhibited strain hardening instability zone (7.8% strain before necking) compared to hot-rolled process (0% strain before necking). On the other hand, Q&P process highly decreased strain hardening instability zone (0.77% strain before necking) compared to hot-rolled process (3.4% strain before necking).

Keywords Carbon steel · Hot-rolled · Quenching after martensitic finish · Quenching and partitioning · Mechanical properties · Strain hardening instability

1 Introduction

Mechanical properties of carbon steels are strongly dependent on their microstructure obtained after heat treatments that are generally performed in order to achieve a good hardness and/or tensile strength with sufficient ductility [1]. Due to their excellent overall performance, low and medium carbon steels have widely used in fundamental fields such as machine manufacturing, energy development, and rail traffic [2–4]. Recently, there has been an intense focus on the improvement of mechanical properties of low and medium carbon steels using deformation technologies such as forging, hot rolling, cold rolling, and thermomechanical processes [5, 6]. Retained austenite (RA) in carbon steels has been examined extensively due to its complex influences on the components service [7, 8]. Many studies appeared

✉ Ramadan N. Elshaer
ramadan_elshaer@yahoo.com

Mohamed K. El-Fawakhry
abdrabu1979kamal@yahoo.com

Ahmed I. Z. Farahat
ahmedzaky61@yahoo.com

[1] Mechanical Engineering Department, Tabbin Institute for Metallurgical Studies (TIMS), Cairo, Egypt

[2] Steel and Ferroalloys Department, Central Metallurgical Research and Development Institute (CMRDI), Cairo, Egypt

[3] Metals Technology Department, Central Metallurgical Research and Development Institute (CMRDI), Cairo, Egypt

that RA could enhance ductility, and toughness of carbon steels via delaying crack propagation [9, 10]. So, martensitic steels that contain large amounts of RA could exhibit high strength, ductility, and toughness [11]. To benefit from these properties, quenching and partitioning (Q&P) treatment have been developed by Speer et al. [12]. Q&P steel is an expression used to characterize a series of C–Si–Mn, C–Si–Mn–Al, or other steels undergo the lately developed Q&P heat-treatment process. It has wider potential and may be prolonged to other applications and products in the near future. Q&P steel is heat-treated by an initial partial or full austenitization and subsequently followed by a quench to a temperature intermediate between the martensitic start (M_s) and martensitic finish (M_f) temperatures and tentatively maintaining it there (one-step) or at a higher temperature (two-step) to allow carbon of escape from the super-saturated martensite inside the neighboring untransformed austenite. The partitioning of carbon reduces the Ms of untransformed austenite to a value below ambient temperature [13]. Thereafter, steel is quenched to ambient temperature to gain a complex microstructure that contains ferrite, carbon-exhausted martensitic matrix, and a large amount of carbon-enriched retained austenite (RA). So, Q&P steel shows excellent overall mechanical properties with compositions identical to transformation induced plasticity (TRIP) steel, which allows its use in a novel generation of advanced high strength steels (AHSS) for the manufacturing of automotive structures. Numerous researchers [14–26] have studied the relationship between microstructure and mechanical properties of low and medium Q&P steels and exhibited that high strength of Q&P steels results from lath martensite, while its good ductility is referred to as TRIP-aided behavior of retained austenite during quenching and partitioning. Farahat et al. studied the influence of skin pass design on steel sheet surface characteristics [27] and found that the minimum strain hardening exponent ($n = 0.198$) is at 3% skin pass ratio and maximum total elongation pct. Especially, QAM_f and Q&P on the microstructure, mechanical properties, and strain hardening instability of low and medium carbon steels need more investigations. So, the present study investigates the effect of QAM_f or Q&P on the microstructure, mechanical properties, and strain hardening instability of low and medium carbon hot-rolled steels.

2 Experimental Work

The steels used in this study were a hot rolled 0.16C–0.27Si–1.47Mn–0.02Al (low carbon) and 0.49C–0.3Si–0.9Mn–0.03Al (medium carbon) steels. Two heats of carbon steel (0.16 and 0.49 wt% carbon) were cast as plates by sand casting technique. Melting process was done using medium frequency in an open atmosphere induction furnace and cooled in a sand mold. The chemical composition of the steels was analyzed using a foundry-master pro spectrometer (OXFORD instrument, Germany). The detailed chemical compositions of the steels are listed below in Table 1. In these low and medium carbon steels, silicon was added to suppress the formation of cementite [8], while manganese was added to stabilize austenite and minimize the Ms value [28]. The carbon steel samples with 100 × 40 × 30 mm dimensions were cut and prepared from the as-cast plates using CNC machine for hot rolling process. The samples were hot-rolled at 1200 °C for 30 min followed by air cooling as shown in Fig. 1. The hot-rolled samples were then passed over a series of 6 passes down to a final thickness of 15 mm. After each pass, the sample was then heated to 1200 °C for 10 min in air before being rolled again. Small samples for dilatation testing were machined with Φ5 × 20 mm. A dilatometer attached with a computer-controlled horizontal pushrod dilatometer (LINSEIS DIL L75 Platinum Series instrument, Germany), was used for measuring the characteristic temperatures for selecting the parameters of the critical transformation temperatures.

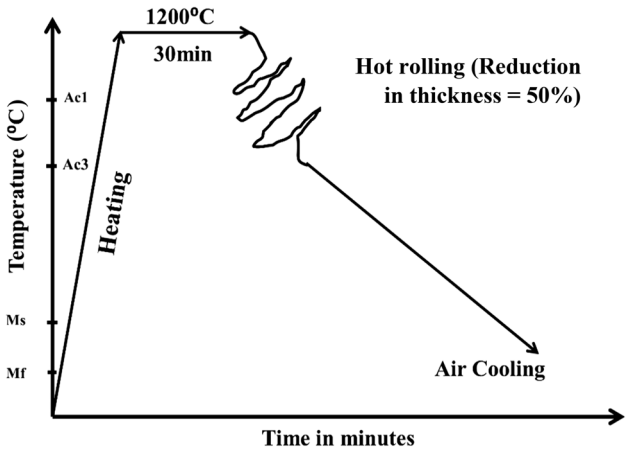

Fig. 1 Hot rolling process

Table 1 Chemical composition of the hot rolled steels (mass fraction, %)

Alloy	C	Si	Mn	P	S	Al
0.16C	0.155	0.267	1.47	0.0168	0.0077	0.021
0.49C	0.486	0.299	0.908	0.014	0.005	0.026

Heating and cooling rates of dilatometer testing were 20 °C /min. Heating up was done till 1200 °C while cooling down was till room temperature. Two different heat treatment processes (QAM_f and Q&P) were applied in this study, Fig. 2. The first heat treatment of low carbon steel (0.16C) was heating up to intercritical annealing zone (830 °C) followed by quenching in a salt bath after martensitic finish (160 °C). The second one was heating above Ac_3 (830 °C) followed by quenching in salt bath after martensitic start (160 °C). To investigate the microstructure after hot rolling and heat treatment processes, samples were cut and prepared using standard methods for polishing and nitric etching. After that, microstructure characteristics were investigated using Quanta-FEI/FEG-250 field emission scanning electron microscope (FESEM). Hardness measurements were conducted by Vickers hardness tester. Seven readings were taken on each sample and the average was recorded. Tensile testing was carried out for machined samples with a diameter and gage length of 9 and 45 mm, respectively. Tensile testing was obtained according to three repeated testing results.

3 Results and Discussion

3.1 Dilatation Analysis

The dilatation curve is a powerful tool to determine and analyze the actual critical transformation temperatures during continuous heating or cooling process [29]. Figure 3 shows the general dilatation behavior of Alloy 0.16C during the continuous heating and cooling steps. The first derivative of dilatation exemplifies not only the total transformation behavior but also shows distinct characteristics of each phase that existed [29]. To understand the features of each phase

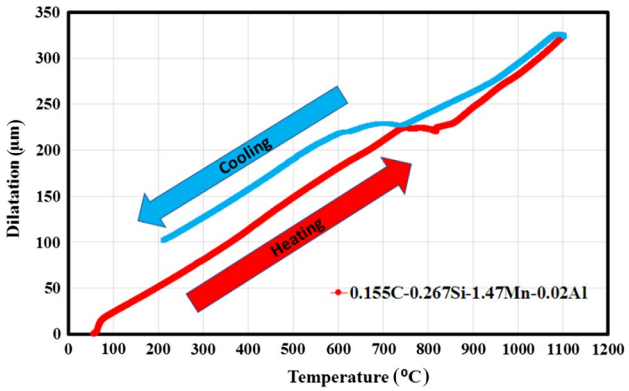

Fig. 3 Dilatation curve in general (showing continuous heating and cooling paths) of Alloy 0.16C

using the first derivative of dilatation with temperature, Liu et al. studied distinguishing oneself ferrite transformation behaviors [29] and observed changes in slope due to great inhomogeneous austenite grain size during ferrite transformation. Figure 4 represents the first derivative behavior for Alloy 0.16C during continuous heating; it seems clear that Ac_1 and Ac_3 are 736 and 870 °C, respectively. The Ac_1 and Ac_3 zone exhibits three deep convexes which represent ferrite transformation inside grains or at the grain boundaries.

The first derivative of dilatation during cooling shows the constant level in the area of no transformation and is convex in shape during transformation [29]. The first derivative of dilatation showed two-stage transformations. The first peak was due to interface-controlled ferrite formation in large grains and the second was due to diffusion-controlled ferrite formation in small grains. Figure 5 illustrates the first derivative of dilatation; it shows the critical transformation temperature Ar_3 and Ar_1 during continuous cooling of 760

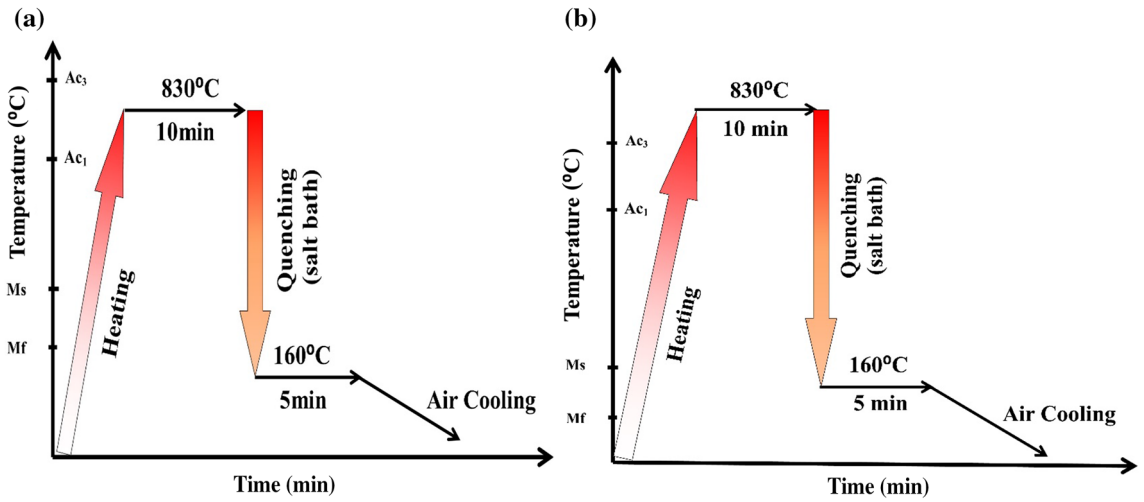

Fig. 2 Heat treatment processes **a** 0.16C (QAM_f) and **b** 0.49C (Q&P)

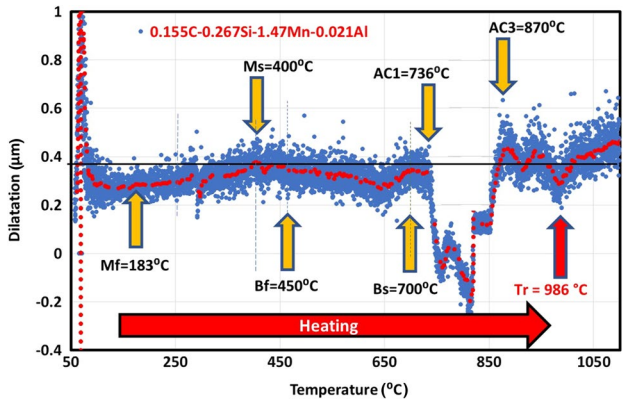

Fig. 4 First derivative heating curve for Alloy 0.16C

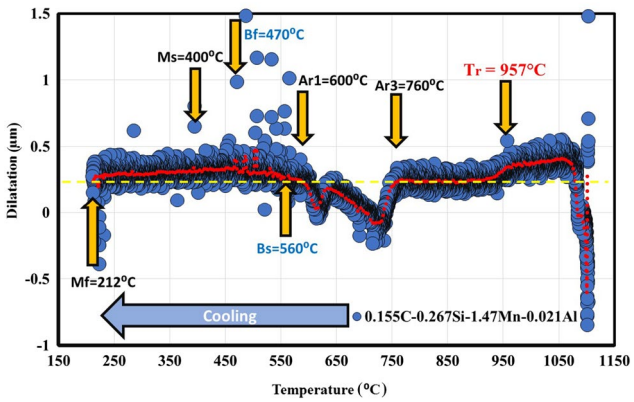

Fig. 5 First derivative continuous cooling curve for Alloy 0.16C

and 600 °C respectively. The Ar_1 and Ar_3 give two convexes. Furthermore, bainite transformation temperatures (B_s & B_f) are 560 and 470 °C, respectively. However, martensite phase temperatures (M_s & M_f) are 400 and 212 °C, respectively. Bainite and martensite phases provide joint concave. Recrystallization (T_r) phenomena appears during continuous heating and cooling of 986 and 957 °C, respectively.

Figure 6 demonstrates the general dilatation behavior of Alloy A (0.49C). To determine the actual transformation temperature during continuous heating or cooling, the first derivative for heating or cooling was conducted separately as seen in Figs. 7 and 8. From dilatation curve, it was clear that continuous heating and cooling rates equal to 20 °C/min. It is very essential to determine the critical transformation temperatures Ac_1 and Ac_3 to perform hot rolling process at proper temperature and to start any heat treatment process at significant temperatures. From dilatation curve of Fig. 7, it is obvious that Ac_1 and Ac_3 during continuous heating (deep convex) were 717 and 780 °C, respectively. While during continuous cooling, Ar_3 and

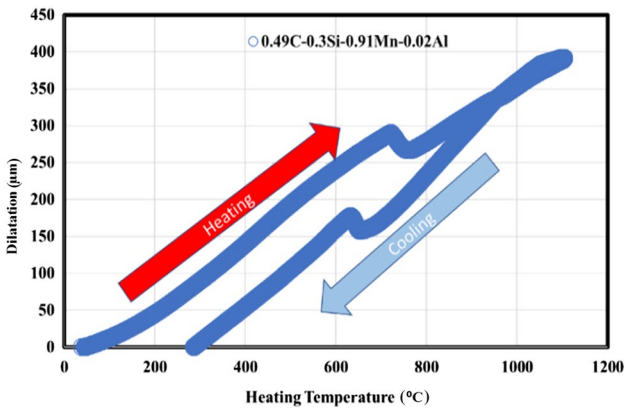

Fig. 6 Dilatation curve in general (showing continuous heating and cooling paths) of Alloy 0.49C

Ar_1 (Fig. 8) decreased to be 716 and 615 °C, respectively. To carry out proper heat treatment cycles of Dual-Phase, TRIP, TRIPLEX, and Advanced High Strength Steels it is necessary to determine the critical transformation temperatures such as Bainite (B_s & B_f) and Martensite (M_s&M_f) during continuous cooling. The Martensite phase started to decompose during continuous heating at nearly room temperature (38 °C) and continued to 383 °C (M_f). First derivative curve shows after martensite decomposition finishing convex bainite phase (during heating) which directly started to decompose at 470 °C (B_f) and continued to 650 °C (B_s). It is interesting to note that the dilatometer behavior shows shallow convex between 900 and 1000 °C temperatures which is expected as Recrystallization zone. Recrystallization temperature (T_r) appears during continuous heating and cooling of 965 and 951 °C, respectively.

During continuous cooling, critical transformation temperatures Ar_3 and Ar_1 decreased to be 716 and 615 °C, respectively. Also, Bainite transformation temperatures (B_s & B_f) decreased than heating step to 587 and 482 °C, respectively. Martensite phase temperatures (M_s & M_f) were 382 and 120 °C, respectively. The dilatation behavior at the martensitic zone shows strong behavior at the end of dilatation curve (left side) giving indication that martensite finished at 120 °C. Table 2 summarizes the critical transformation temperatures for low and medium carbon steels during continuous heating and cooling steps.

Figure 9 demonstrates the martensitic start and finish (M_s & M_f) temperatures. To emphasize the accuracy dilatation behavior for 0.16 and 0.49 wt% carbon steels, the martensitic start (M_s) and finish (M_f) diagram is used to compare with the dilatation analysis for 0.16 and 0.49 wt% carbon steels used in this study. The martensitic points show well-fitness with the general trend. It is also clear that at 0.16 wt% carbon steel, the martensitic transformation starts at approximately the same level for low carbon steel one. On the other hand,

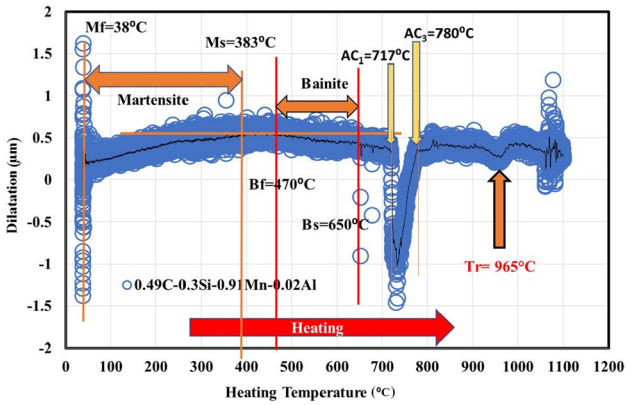

Fig. 7 First derivative continuous heating curve for Alloy 0.49C

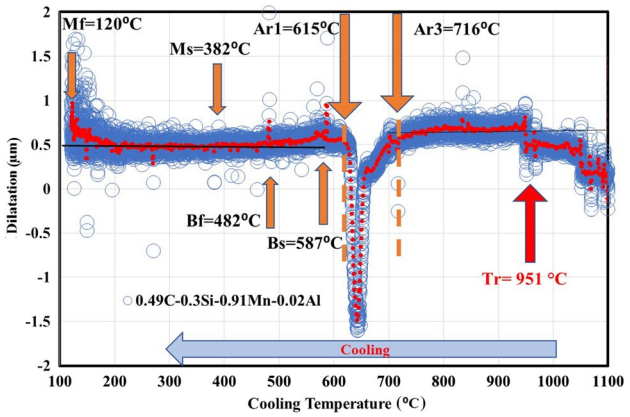

Fig. 8 First derivative continuous cooling curve for Alloy 0.49C

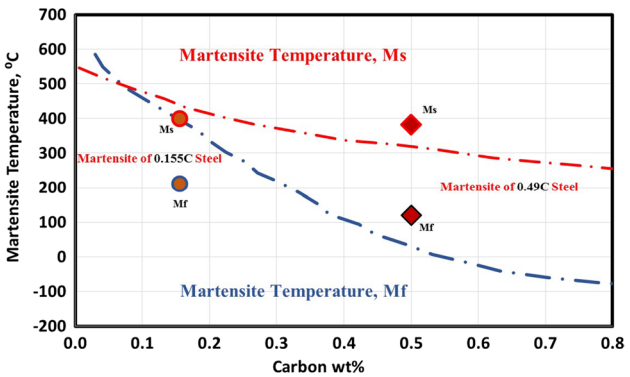

Fig. 9 Martensitic start and finish temperature for steel (0.16 and 0.49 wt% carbon) [30]

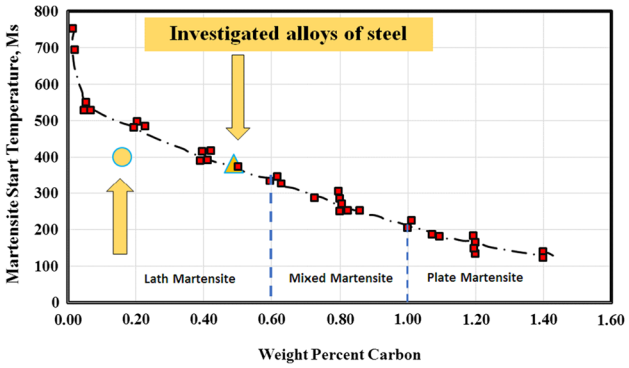

Fig. 10 Martensitic start temperatures (M_s) as a function of carbon content in steels [30]

martensitic transformation of 0.16 wt% carbon steel early finishes before 0.49 wt% carbon steel one due to increasing carbon.

Figure 10 compares actual martensitic start temperature deduced from dilatation testing with literature results [30]. It seems clear that at 0.49 wt%C steel the dilatometric results completely coincide with literature [30]. However, at 0.16 wt%C steel, the dilatometric results do not coincide with literature [30] and the difference is approximately 100 °C. Figure 11 shows bainite start temperature (0.16C steel) coincides with dilatometric results while bainite finish temperature slightly extends to 380 °C. However, for 0.49 wt%C steel, bainite start temperature of dilatometric shows approximately 60–20 °C depending upon continuous cooling rates. Martensitic start temperature (0.16C steel) shows complete agreement while for 0.49 wt%C steel there is gap between literature CCC curve [31] and dilatometric results (80 °C). For both types of steels, martensitic finish temperatures show difference ranging from 60 to 170 °C.

Table 2 Actual critical transformation temperatures, °C

Alloy	Ac_1	Ac_3	Ar_1	Ar_3	B_s	B_f	M_s	M_f	T_r
0.16C	736	870	600	760	560	470	400	212	986
0.49C	717	780	615	716	587	482	382	120	965

3.2 Microstructure Evolution

3.2.1 Microstructure of 0.16 wt% Carbon Steel

Figure 12 shows coarse bands structure of ferrite (dark) and pearlite (grey) as well as small amount of retained austenite for 0.16 wt% hot rolled carbon steel. The pearlite itself consists of bands (or lamellar structure) of ferrite and cementite (Fe_3C) which is formed by the eutectoid decomposition of austenite upon cooling. Furthermore,

the ferritic matrix can be described as connected matrix, as shown in FESEM image, Fig. 12. The treated samples at 830 °C were in intercritical annealing zone of the two-phase area (i.e. ferrite and austenite). After QAM_f process, the microstructure consists of bainite, ferrite, retained austenite, and lath martensite, Fig. 13. During the transformation of austenite to bainitic ferrite (BF), carbon diffused to austenite resulting in stabilization of

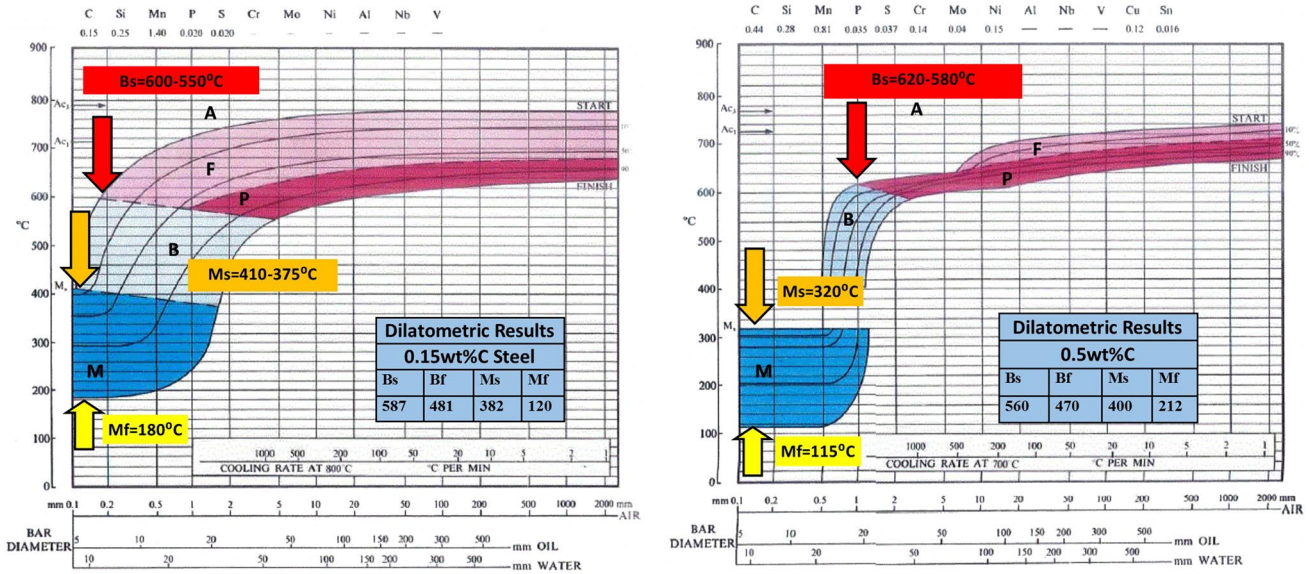

Fig. 11 Continuous cooling curve (CCC) of 0.16 and 0.49C steels [31]

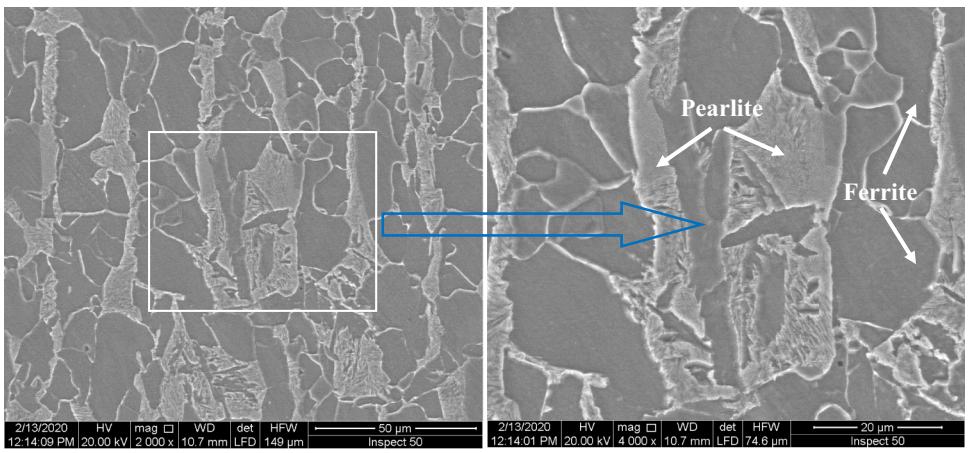

Fig. 12 FESEM microstructure of 0.16 wt% carbon steel (hot rolled), coarse banded structure

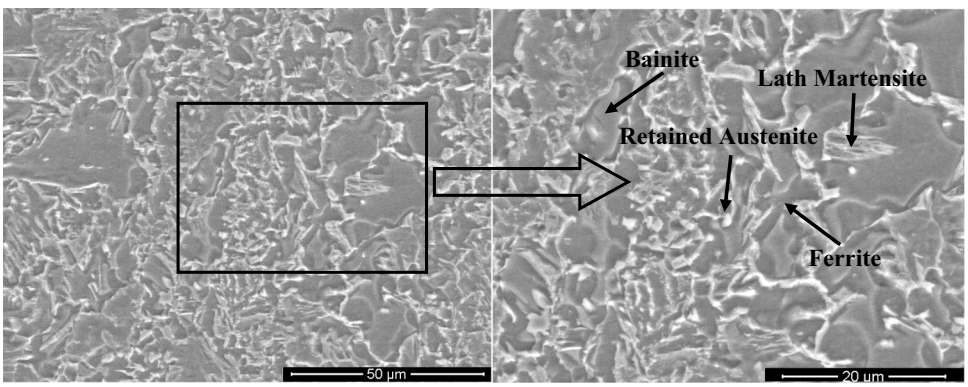

Fig. 13 FESEM microstructure (Bainite-Lath Martensite-Retained Austenite–Ferrite) of 0.16 wt% carbon steel (QAM_f), fine structure

the austenite. The volume fraction of transformed bainitic ferrite reached approximately 70% which was estimated using image analysis software. Small nodules of retained austenite and low amount of lath martensite are found.

3.2.2 Microstructure of 0.49 wt% Carbon Steel

Figure 14 shows coarse pearlite islands surrounded by ferrite phase for 0.49 wt% hot rolled carbon steel. The treated samples at 830 °C were above A_{C3}. The microstructure of trade Q&P steels basically consists of martensite (70%–80%) formed during quenching, ferrite (10%–20%) formed from the austenite phase during slow cooling, and dispersed retained austenite (5%–10%) stabilized by carbon enrichment during partitioning. FESEM micrographs (Fig. 15) of medium carbon steel (0.49 wt%C) after Q&P shows actual polygonal ferrite is 20%, lath martensite is 72% (Fig. 16), and low amount of retained austenite (RA) is 8%.

3.3 Hardness

Figure 17 shows hardness variation of low and medium carbon steels after hot-rolled and heat-treated processes. In low carbon steel (0.16C), the results appeared an insignificant variance in the sample hardness after the QAM_f process compared to the hot-rolled sample where the hardness decreases from 205 to 186 HV_{10} (−9%) due to the change of microstructure (from ferrite pearlite to ferrite-bainite-martensite). However, in medium carbon steel (0.49C), the results showed obvious difference in the sample hardness after the Q&P process compared to the hot-rolled process where the hardness increases from 240 to 390 HV_{10} (+62.5%) due to the presence of a high amount of martensite (72%).

3.4 Tensile Properties

Figure 18 illustrates the selected engineering and true stress–strain curves obtained for low carbon steel (0.16C). QAM_f process increased uniform elongation from 6.6 to 13.5% (+105%) compared to hot rolled process due to the presence of a high amount of bainite. Also, it improved

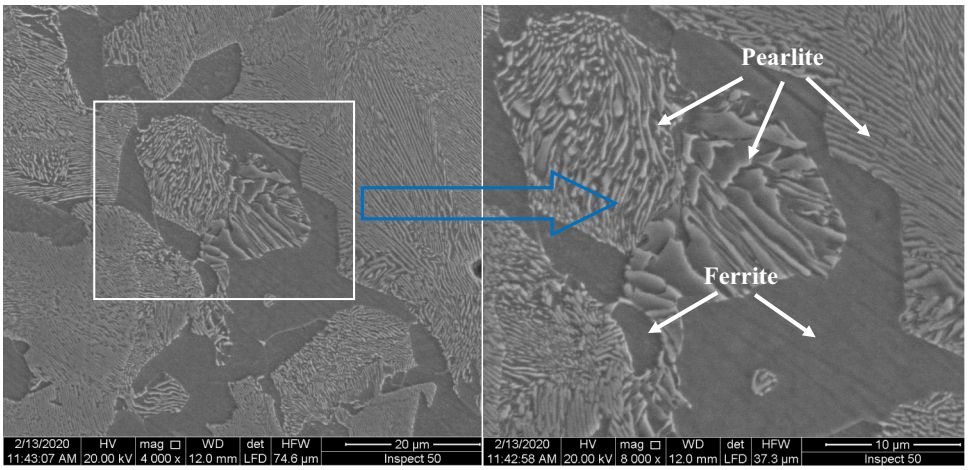

Fig. 14 FESEM microstructure (Pearlite and Ferrite) of 0.49 wt% carbon steel (hot rolled)

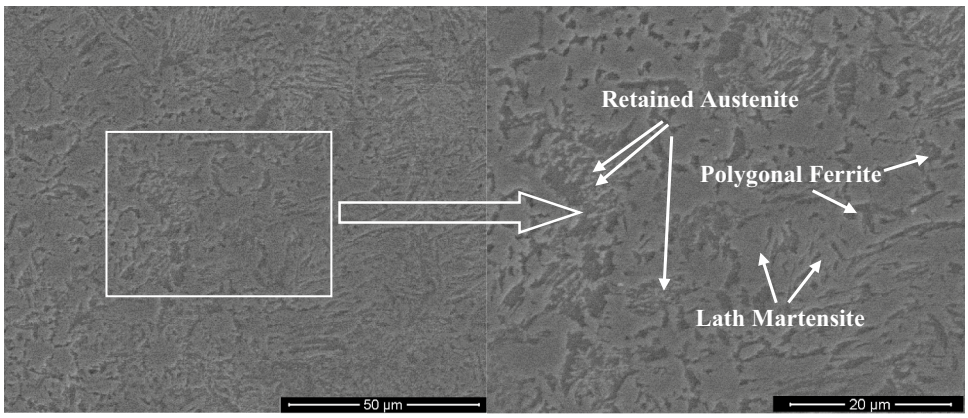

Fig. 15 FESEM microstructure (Lath Martensite, Retained Austenite and Ferrite) of 0.49 wt% carbon steel (Q&P)

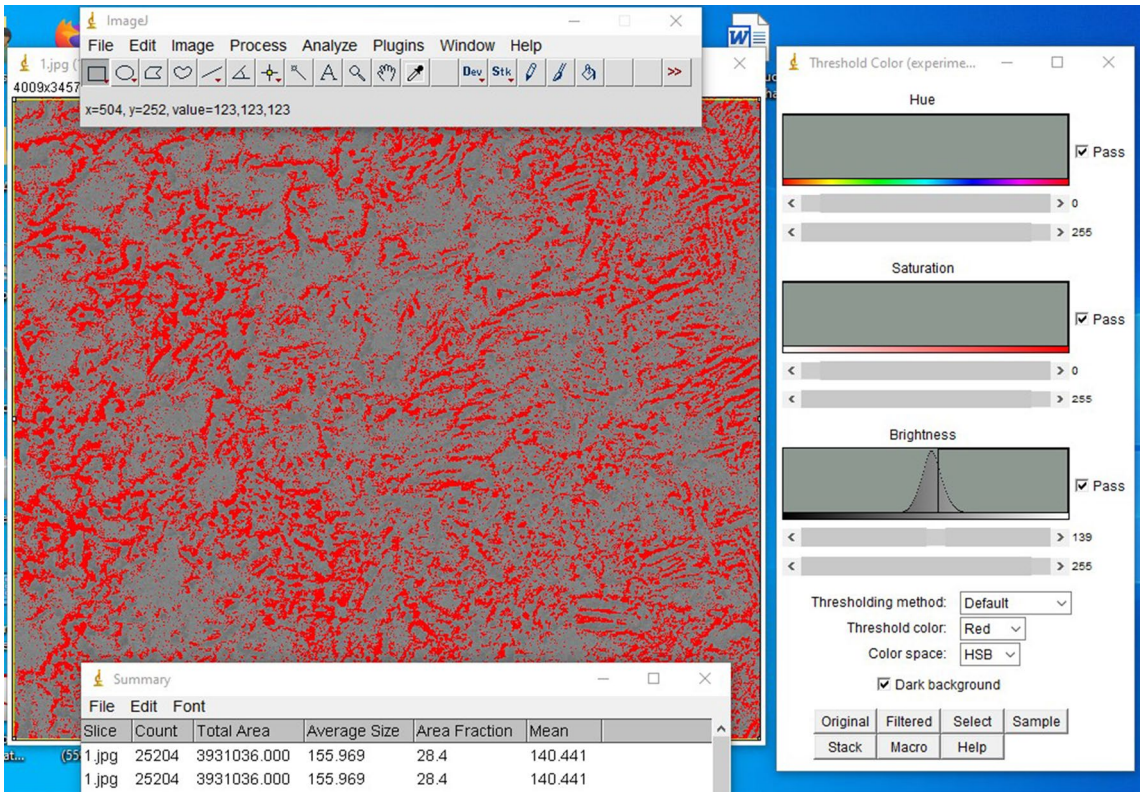

Fig. 16 Volume fraction of martensite (72%) for 0.49 wt% carbon steel (Q&P)

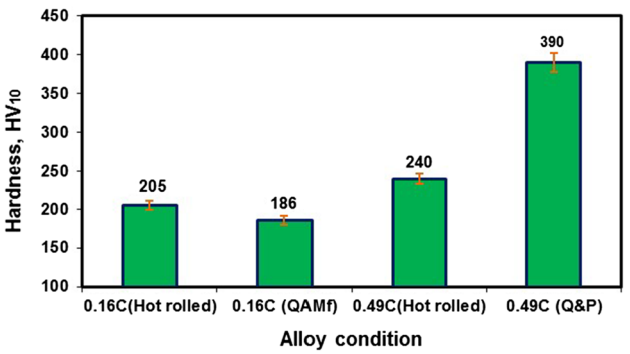

Fig. 17 Hardness of the investigated low and medium carbon steels at different conditions

slightly the ultimate tensile strength (UTS) of 692 MPa. In 0.16C steel, the tensile curve exhibits relatively high slope. From strain hardening exponent (n), it is clear that material after QAM_f undergoes three stages, (see Fig. 19b). The first stage where the material shows strain accumulation of strain hardening exponent (n) equals 0.13 during to deformation process. While the second stage the material exhibits phase transformation (induced martensite) where strain hardening exponent (n) increases to be 0.21. The final stage before necking (BN) at 7.4% uniform strain starts where the strain hardening exponent (n) decreases to 0.1 value.

The low carbon steel (0.16C) after hot rolling shows low strain hardening exponent ($n = 0.05$). On the other hand, after QAM_f the low carbon steel (0.16C) gives relatively high initial strain hardening exponent ($n_{initial} = 0.13$) due to relatively low yield strength (YS/UTS = 0.69). It is obvious that strain hardening exponent ($n_{max} = 0.21$) increases due to induced martensitic transformation. However, at a critical uniform strain (7.4%), the low steel (0.16C) exhibits decreased strain hardening exponent ($n = 0.18$) and continuously decreases to be 0.1. After 7.4% uniform strain (7.8% strain before necking) the steel shows instability of strain hardening exponent (n). QAM_f process increased relatively ultimate strength, elongation, and strain hardening exponent (n) at the expense of yield strength than hot rolled process. Also, QAM_f process increased work hardening instability zone. It produces the strain hardening instability zone (7.8% strain before necking) while hot rolling process gives zero strain hardening instability before necking.

Figure 20 shows the selected engineering and true stress–strain curves acquired for medium carbon steel (0.49C). Q&P decreased uniform elongation from 12.4 to 4.8% (−61%) due to relatively high carbon (0.49 wt%) which generates martensite. However, increased ultimate tensile

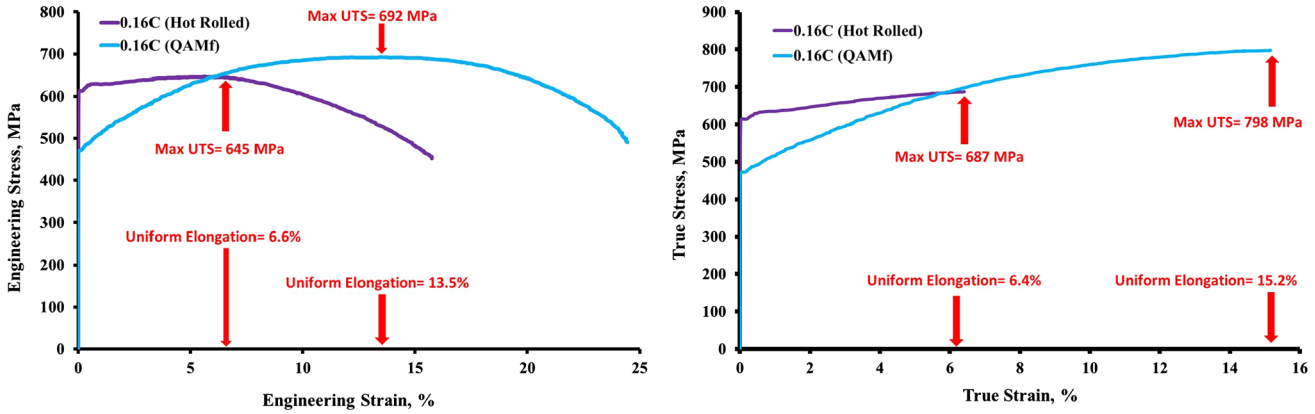

Fig. 18 Engineering and true stress–strain curves of low carbon steel (0.16C) after hot rolling and QAM_f processes

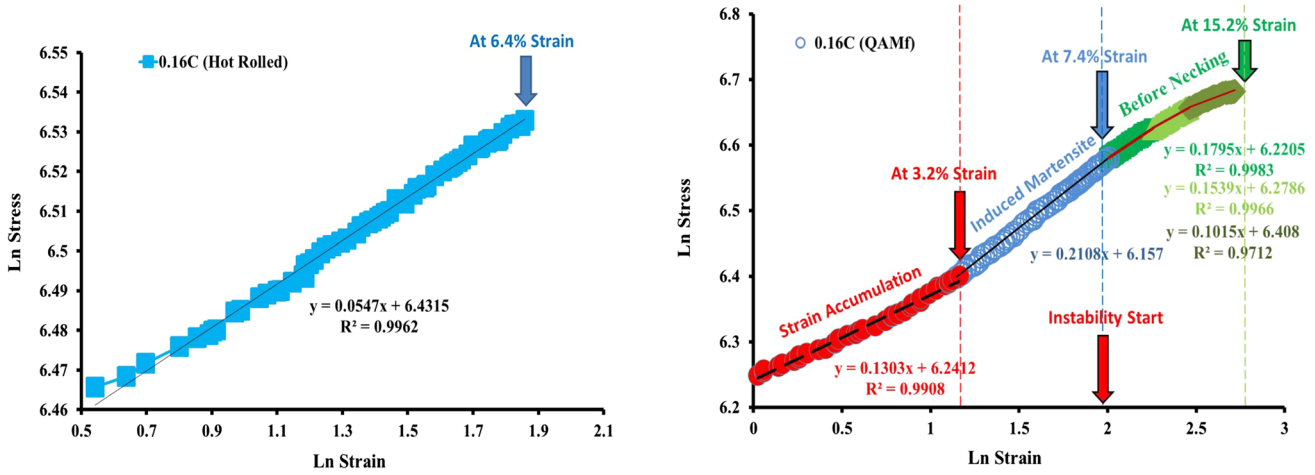

Fig. 19 Strain hardening exponent (n) of low carbon steel (0.16C) after hot rolling and QAM_f processes

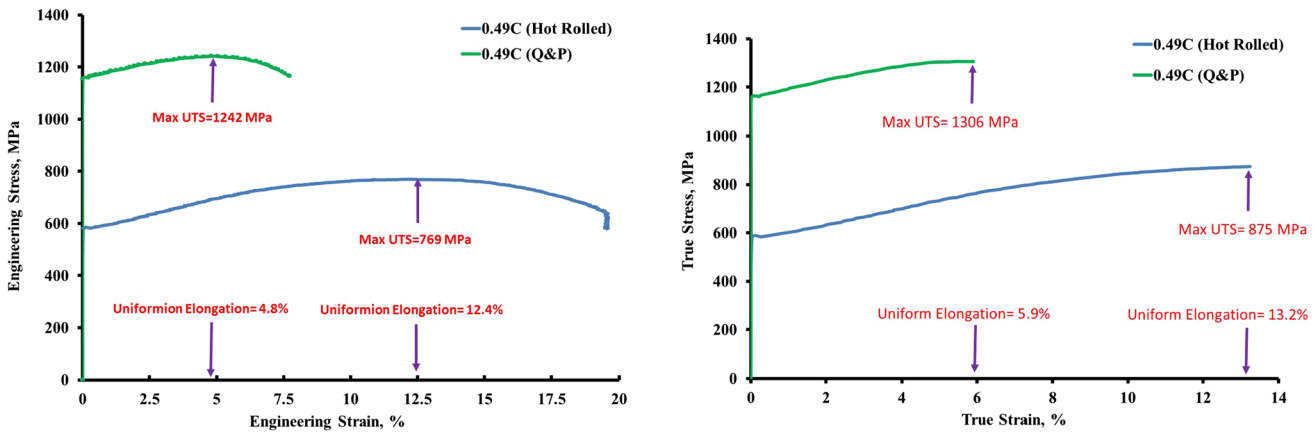

Fig. 20 Engineering and true stress–strain curves of medium carbon steel (0.49C) after hot rolling and Q&P

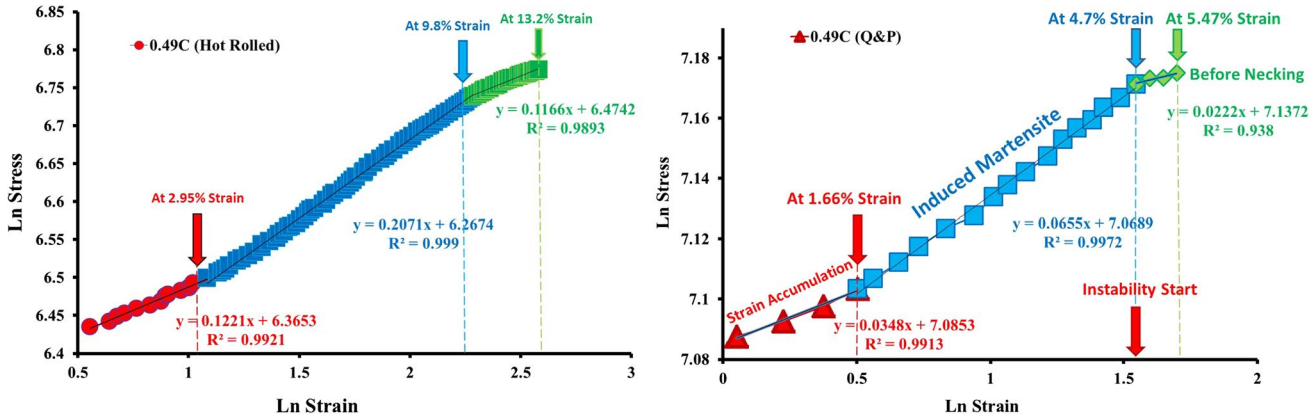

Fig. 21 Strain hardening exponent (n) of medium carbon steel (0.49C) after hot rolling and Q&P processes

Table 3 Tensile and hardness results for low and medium carbon steels

Alloy	Yield strength (MPa)	Ultimate strength (MPa)	Uniform elongation (%)	Total elongation (%)	Hardness (HV_{10})
0.16C (hot rolled)	629	645	6.6	16	205
0.16C (QAM_f)	475	692	13.5	25	186
0.49C (hot rolled)	575	769	12.4	20	240
0.49C (Q&P)	1150	1242	4.8	8	390

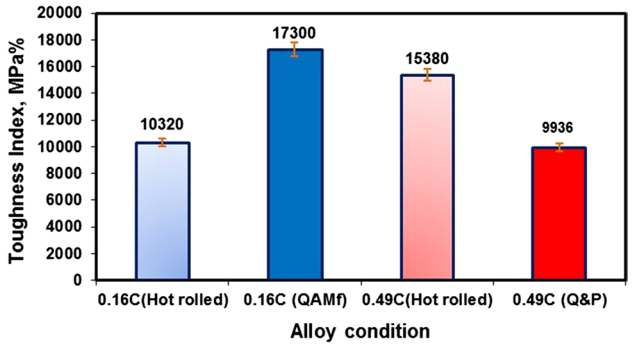

Fig. 22 Toughness index of low and medium carbon steels at different conditions

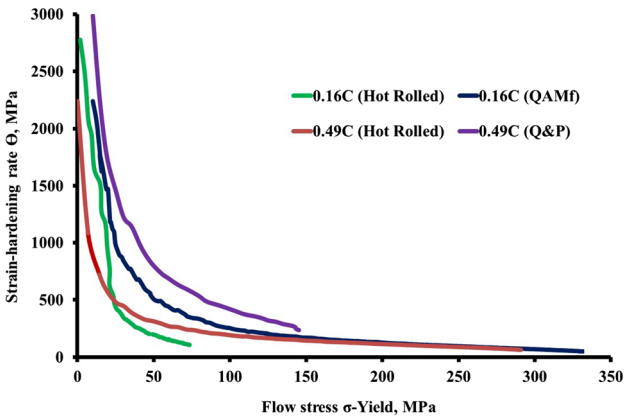

Fig. 23 Kocks-Mecking plots of low and medium carbon steels at different conditions

strength (UTS) from 769 to 1242 MPa (61.5% increase) due to the presence of a high amount of lath martensite (72%) and a low amount of retained austenite (8%) in its structure. In 0.49C steel, tensile curve shows a low slope due to heat treatment transformation, (see Fig. 21). In medium carbon steel, clearly, the strengths (i.e. yield strength (YS) and ultimate tensile strength (UTS)) were increased at the expense of ductility reduction. Further details of tensile properties and hardness for low and medium carbon steels are listed in Table 3. Figure 22 shows the toughness index (TI) for low and medium carbon steels after hot rolling and heat-treating processes. The optimal TI appears at 17,300 MPa% for QAM_f samples. However, the lowest TI is 9936 MPa% for Q&P samples (43% of QAM_f). Figure 23 presents the Kocks-Mecking plots for low and medium carbon steels after hot rolling and heat-treating processes. The strain hardening rate decreases with increasing the flow stress.

The medium carbon steel (0.49C) after hot-rolled process exhibits high initial strain hardening exponent ($n = 0.12$). However, it increases to be ($n = 0.21$) and decreases again to be ($n = 0.12$) before necking. So, the hot-rolled steel starts its strain hardening instability at 9.8% (3.4% strain before

necking). Furthermore, after Q&P the medium carbon steel (0.49C) gives relatively low initial strain hardening exponent ($n_{initial} = 0.03$) due to relatively high yield strength (YS/UTS = 0.93). It is clear that strain hardening exponent ($n_{max} = 0.06$) increases due to induced martensitic transformation. Moreover, the medium carbon steel decreased strain hardening exponent ($n = 0.02$) at 5.47% strain (0.77% strain before necking). Q&P process enhanced both yield and ultimate strengths at the expense of elongation and strain hardening exponent (n). Also, Q&P process decreased strain hardening instability zone. It produces the strain hardening instability zone (0.77% strain before necking) while hot-rolled process gives the strain hardening instability zone (3.4% strain before necking).

In summary, QAM_f process increased strain hardening instability zone (7.8% strain before necking) compared to hot-rolled process (0% strain before necking). However, Q&P process decreased strain hardening instability zone (0.77% strain before necking) compared to hot-rolled process (3.4% strain before necking).

4 Conclusions

The investigated low and medium hot rolled carbon steels were heat-treated using QAM_f and Q&P processes. Microstructure evolution, mechanical properties, and strain hardening instability of hot-rolled, and heat-treated samples were reported. Hence, this work can be concluded in the following points:

1. Microstructure of 0.16C hot rolled steel; it gives coarse banded structure of ferrite, pearlite, and small amount of retained austenite. However, after QAM_f process, the microstructure consists of bainite, lath martensite, retained austenite, and ferrite.
2. Microstructure of 0.49C hot rolled steel; it consists of coarse pearlite islands surrounded by ferrite phase. While, after Q&P shows polygonal ferrite, lath martensite, and retained austenite.
3. Critical transformation temperatures of 0.16 wt% carbon steel were found of $Ac_1 = 736$ and $Ac_3 = 870$ °C. While, at 0.49 wt% carbon steel of $Ac_1 = 717$ and $Ac_3 = 780$ °C. Bainitic transformation temperatures ($B_s = 560$ & $B_f = 470$ °C) at 0.16 wt% carbon steel slightly decrease compared with 0.49 wt% carbon steel ($B_s = 587$ & $B_f = 481$ °C).
4. Start martensitic transformation temperature (M_s) is approximately the same at 0.16 wt% (400 °C) and 0.49 wt% carbon steels (382 °C). On the other hand, the finish martensitic transformation temperature (M_f) highly decreases at 0.49 wt% carbon steel (120 °C) compared to 0.16 wt% carbon steel (212 °C).
5. In low carbon steel (0.16C), QAM_f process increased uniform elongation from 6.6 to 13.5% (+105%). Also, it improved slightly the UTS (+7%). Yield strength decreased after QAM_f (−24.5%) while hardness decreased (−7%).
6. In medium carbon steel (0.49C), Q&P process decreased uniform elongation from 12.4 to 4.8% (−61%). However, its increased yield strength from 575 to 1150 MPa (+100%), ultimate tensile strength (UTS) from 769 to 1242 MPa (+61.5%) and hardness from 240 to 390HV (+62.5%).
7. QAM_f process relatively increased ultimate strength, elongation and strain hardening exponent (n) at the expense of yield strength and hardness than hot rolling process.
8. Q&P process enhanced both yield and ultimate strengths at the expense of elongation and strain hardening exponent (n) than hot rolling process.
9. QAM_f process exhibited strain hardening instability zone (7.8% strain before necking) compared to hot rolling process (0% strain before necking). However, Q&P process highly decreased strain hardening instability zone (0.77% strain before necking) compared to hot rolling process (3.4% strain before necking).

References

1. N. Saeidi, M. Jafari, J.G. Kim, F. Ashrafizadeh, H.S. Kim, Met. Mater. Int. **26**, 168 (2020)
2. Z. Changle, F. Hanguang, M. Shengqiang, Y. Dawei, L. Jian, X. Zhenguo, L. Yongping, Mater. Res. Express **6**, 086581 (2019)
3. F. Zhang, Y. Yang, Q. Shan, Z. Li, J. Bi, R. Zhou, Materials **13**, 172 (2020)
4. J.-K. Hwang, Met. Mater. Int. **26**, 603 (2020)
5. H.L. Kim, S.H. Bang, J.M. Choi, N.H. Tak, S.W. Lee, S.H. Park, Met. Mater. Int. **26**, 1757 (2020)
6. K. Sugimoto, S. Sato, J. Kobayashi, A.K. Srivastava, Metals **9**, 1066 (2019)
7. Y.X. Zhou, X.T. Song, J.W. Liang, Y.F. Shen, R.D.K. Misra, Mater. Sci. Eng. A **718**, 267 (2018)
8. Y. Lu, J. Yang, J. Xu, Z. Guo, J. Gu, Heat Treat. Surf. Eng. **1**, 87 (2019)
9. G. Gao, H. Zhang, X. Gui, P. Luo, Z. Tan, B. Bai, Acta Mater. **76**, 425 (2014)
10. B. Bai, G. Gao, X. Gui, Z. Tan, Y. Yeng, Heat Treat. Surf. Eng. **1**, 63 (2019)
11. J. Zhang, H. Ding, R.D.K. Misra, Mater. Sci. Eng. A **636**, 53 (2015)
12. J. Speer, D.K. Matlock, B.C. De Cooman, J.G. Schroth, Acta Mater. **51**, 2611 (2003)
13. D.P. Koistinen, R.E. Marburger, Acta Metall. **7**, 59 (1959)
14. M.J. Santofimia, L. Zhao, R. Petrov, J. Sietsma, Mater. Charact. **59**, 1758 (2008)
15. C.Y. Wang, J. Shi, W.Q. Cao, H. Dong, Mater. Sci. Eng. A **527**, 3442 (2010)
16. E. Abbas, Q. Luo, D. Owens, Acta Metall. Sin. **32**, 74 (2019)

17. M.V. Karavaeva, S.K. Nurieva, N.G. Zaripov, A.V. Ganeev, R.Z. Valiev, Met. Sci. Heat Treat. **54**, 155 (2012)
18. J. Tian, G. Xu, Z. Jiang, H. Hu, Q. Yuan, X. Wan, Met. Mater. Int. **26**, 961 (2020)
19. L. Wang, J.G. Speer, Metallogr. Microstruct. Anal. **2**, 268 (2013)
20. M.V. Karavaeva, S.K. Kiseleva, M.M. Abramova, A.V. Ganeev, R.Z. Valiev, IOP Conf. Ser. Mater. Sci. **63**, 012056 (2014)
21. Y. Tian, H. Wang, Y. Li, Z. Wang, G. Wang, Mater. Res. **20**, 853 (2017)
22. H.F. Lan, L.X. Du, R.D.K. Misra, Mater. Sci. Eng. A **611**, 194 (2014)
23. X.Y. Long, J. Kang, B. Lv, F.C. Zhang, Mater. Design **64**, 237 (2014)
24. A. Grajcar, K. Radwañski, Mater. Tehnol. **48**, 679 (2014)
25. Y. Xu, X. Tan, X. Yang, Z. Hu, F. Peng, D. Wu, G. Wang, Mater. Sci. Eng. A **607**, 460 (2014)
26. X. Tan, Y. Xu, X. Yang, Z. Liu, D. Wu, Mater. Sci. Eng. A **594**, 149 (2014)
27. A.I.Z. Farahat, A.M. Bahgat Gemeal, R.N. Elshaer, J. Fail. Anal. Prev. **16**, 86 (2016)
28. K. Zhang, M. Zhang, Z. Guo, N. Chen, Y. Rong, Mater. Sci. Eng. A **528**, 8486 (2011)
29. Y.C. Liu, F. Sommer, E.J. Mittemeijer, Acta Mater. **54**, 3383 (2006)
30. G. Krauss, *Steels: Processing, Structure and Performance*, 2nd edn. (ASM International, Materials Park, 2015), pp. 68–85
31. M. Atkins, *Atlas of Continuous Cooling Transformation Diagrams for Engineering Steels* (Market Promotion Department, British Steel Corporation, London, 1977), pp. 46–54